https://doi.org/10.5194/ar-2026-29
Preprint. Discussion started: 4 August 2026

AEROSOL Research Discussions

Measurement-Model Closure of Sub-20 nm Particle Charge Fractions under Varying Trace Gas Composition

Fabian Schmidt-Ott[1,2], Robert Nishida[3,4], Sebastian Schmitt[5], Jason Olfert[6], George Biskos[2,7], Juha Kangasluoma[1]

[1]Institute for Atmospheric and Earth System Research, University of Helsinki, 00014, Helsinki, Finland
[2]Climate & Atmosphere Research Centre, The Cyprus Institute, 2121 Nicosia, Cyprus
[3]Department of Mechanical & Mechatronics Engineering, University of Waterloo, Waterloo, Ontario, Canada
[4]Atmose Ltd, Edmonton, Alberta, Canada
[5]Institute for Occupational Safety and Health (IFA), German Social Accident Insurance (DGUV), 53757 Sankt Augustin, Germany
[6]Department of Mechanical Engineering, University of Alberta, Edmonton, Alberta, Canada
[7]Faculty of Civil Engineering & Geosciences, Delft University of Technology, Delft, The Netherlands

Correspondence to: F. Schmidt-Ott (fabian.schmidt-ott@helsinki.fi); G. Biskos (g.biskos@cyi.ac.cy); J. Kangasluoma (juha.kangasluoma@helsinki.fi)

Abstract. The sizing of aerosol particles is commonly carried out by electrical techniques, requiring particles to reach a known charge distribution prior to measurement. This is typically achieved by passing the particles through bipolar diffusion chargers, where the resulting steady-state particle charge distribution depends on the properties of the ions therein. We present new measurements of the charge fractions of sub-20 nm particles after bipolar diffusion charging, along with measurements characterizing the properties of ions generated within the bipolar charger. Our results show that, under steady-state conditions, the particle charge distribution is primarily determined by charger ion properties, which can be influenced even by trace gas contamination. Specifically, the use of commonly employed conductive silicone tubing, which emits trace concentrations of volatile methyl siloxanes (VMS), changes the mean positive ion mobility by 20 %, leading to deviations of up to 25 % in the fraction of singly charged particles relative to measurements without the tubing. We further show that the use of conductive silicone tubing stabilizes the mean positive ion mobility to 1.05 ± 0.10 cm^2 V^{-1} s^{-1} associated with VMS. The mobility of the negative ions, on the other hand, remains highly dependent on gas composition. Building on the finding that positive ion properties can be readily stabilized to repeatable values, we show that negative ion properties can be approximated through a simple bipolar Mobility Particle Size Spectrometers (MPSS) measurement. Our measurements show good agreement with charge fractions predicted by Hoppel & Frick theory, with relative differences of up to −6.1 % and 0.6 % for positive and negative charge fractions, respectively, supporting the validity of classical charging theory for sub-20 nm particles. In contrast, significant deviations from the commonly used Wiedensohler (1988) approximation highlight the importance of accounting for environment-specific ion properties when predicting particle charge distributions.

https://doi.org/10.5194/ar-2026-29
Preprint. Discussion started: 4 August 2026

AEROSOL Research Discussions

1 Introduction

The number of charges aerosol particles carry affects many of their properties. The deposition of particles in human airways as well as on filters has been shown to significantly increase with its charge (Hinds, 1999; Melandri et al., 1983; Tu et al., 2016; Vincent, 1985). Furthermore, charging particles can be used to influence particle agglomeration and synthesis (Matsoukas, 1997; Park et al., 2005; Vemury and Pratsinis, 1996). Particle charge also plays a central role in mobility-based measurement techniques such as Mobility Particle Size Spectrometers (MPSS), where particle size is inferred from electrical mobility after establishing a steady-state charge distribution (Knutson and Whitby, 1975). Such mobility-based sizing methods form the basis of standardized procedures for aerosol and nanoparticle characterization (ISO 15900, 2020).

Typically, in MPSS measurement techniques, particles are charged using bipolar diffusion charging, which establishes a steady-state particle charge distribution (Liu & Pui, 1974) by exposing particles to gaseous ions of both polarities. This requires sufficiently high ion concentrations or sufficient ion-particle interaction time (Adachi et al., 1989; De La Verpilliere et al., 2015; Hoppel and Frick, 1990; Ibarra et al., 2020). Bipolar ion sources, such as radioactive materials (e.g., ^{241}Am, ^{63}Ni, ^{210}Po and ^{85}Kr) that emit ionizing radiation, as well as by X-ray radiation or bipolar corona discharge ionization (Lee et al., 2005; Liu et al., 1986; Liu and Pui, 1974; Whitby, 1961) are typically used in this process.

The resulting particle charge distribution can be calculated using the widely accepted diffusion charging theory originally proposed by Fuchs (1963), with a correction of the ion-aerosol collision probability introduced by Hoppel and Frick (1986). The predicted charge distribution depends strongly on the charger ion properties, particularly on their electrical mobility (Z_i) and mass (m_i).

A large range of studies exist pointing out that charger ion properties can significantly vary depending on both the composition of the carrier gas as well as the ionization method used, where the electrical mobility of positive ions (Z_i^+) ranges from 1.0 to 2.0 cm^2 V^{-1} s^{-1} and that of negative ions (Z_i^-) ranges from 1.1 to 2.4 cm^2 V^{-1} s^{-1} (Liu et al., 2020; Schmidt-Ott et al., 2024; Steiner et al., 2014; Tigges et al., 2015). Specifically, the use of conductive silicone tubing has gained much attention, as the outgassing of volatile methyl siloxanes (VMS) from this tubing adds contamination that can significantly change the composition of the carrier gas and therefore influence the charger ion properties (Asbach et al., 2016; Liu et al., 2020; Maißer et al., 2015; Schmidt-Ott et al., 2024; Steiner and Reischl, 2012; Timko et al., 2009).

Besides studies on the ion properties, there have been various studies on measuring particle charge distributions, typically involving a tandem differential mobility analyzer (TDMA) or Aerodynamic Aerosol Classifier (AAC)-DMA setup (Adachi et al., 1985; Biskos et al., 2005; Gopalakrishnan et al., 2015; Hussin et al., 1983; Jiang et al., 2014; Johnson et al., 2020, 2021; Kojima, 1978; Reischl et al., 1983, 1996; Stober et al., 1991; Wiedensohler et al., 1986). A common feature of all

https://doi.org/10.5194/ar-2026-29
Preprint. Discussion started: 4 August 2026

these studies is that the measured charge fractions are compared to those obtained from charging theory, where the ion properties needed as input are left as fitting parameters whose values can, to some extent, be freely chosen. On the other hand, measurements of charger ion properties along with the charge distribution measurement are scarce. Only Li et al. (2025) have measured ion properties along with the charge distribution of 3-100 nm particles, evaluating the effects of the discharge gas, carrier gas and relative humidity (RH) on ion properties and charge fractions, finding that the measured charge fractions can be well described by existing theories.

In the sub-20 nm size range, significant uncertainties exist in MPSS measurements. In this size range, only a small fraction of particles are charged, so even small errors in the assumed charge distribution, arising for example from uncertainties in ion properties, can lead to large uncertainties in the inverted particle concentrations (Kangasluoma et al., 2020; Leppä et al., 2017; Niskanen et al., 2026). For the measurement of these sizes, it is therefore especially important to have accurate information on ion properties, but also to implement those ion properties when determining the particle charge distribution.

In this work, we present measurements of the charge fractions of sub-20 nm particles undergoing bipolar diffusion charging using a novel experimental approach. Considering that multiply charged particles are negligible in this size regime (Wiedensohler, 1988), the need for a TDMA setup is eliminated (Bello et al., 2024), minimizing particle losses and enabling more accurate measurements of sub-20 nm charge fractions than existing methods. Besides the measurement of charge fractions, we simultaneously measured the charger ion properties. By systematically varying these properties and comparing measured and modelled charge fractions, we evaluate both the Hoppel and Frick (1986) charging theory and the widely used approximation proposed by Wiedensohler (1988). Furthermore, we show that charger ion properties, and consequently the resulting particle charge distribution, are sensitive to trace gases present in the carrier gas. Building on this sensitivity, we show that the controlled introduction of specific trace compounds can yield a positive ion population of well-defined properties. We further provide a method to infer the negative ion properties, as an approach to improve the accuracy in determining the gas composition-specific particle charge distribution.

2 Background

2.1 Theoretical model

Bipolar diffusion charging is a stochastic birth-death process that can be described by of the following set of coupled ordinary differential equations (ODE; Marlow and Brock, 1975),

$$\frac{dN_0}{dt} = n_i^+ \beta_{-1}^+ N_{-1} + n_i^- \beta_{+1}^- N_{+1} - n_i^+ \beta_0^+ N_0 - n_i^- \beta_0^- N_0 \quad (1)$$

$$\frac{dN_q}{dt} = n_i^+ \beta_{q-1}^+ N_{q-1} + n_i^- \beta_{q+1}^- N_{q+1} - n_i^+ \beta_q^+ N_q - n_i^- \beta_q^- N_q \qquad |q| \geq 1, \quad (2)$$

https://doi.org/10.5194/ar-2026-29
Preprint. Discussion started: 4 August 2026

AEROSOL Research Discussions

where N_0 and N_q denote the number concentration of neutral and charged aerosol particles, respectively, of any given size carrying q elementary charges (positive or negative); n_i^+ and n_i^- are the positive and negative ion concentrations, respectively; β_q^+ and β_q^- is the combination coefficient of ions of positive or negative charge to particles already carrying q charges.

For sub-20 nm particles, we assume that the presence of multiply charged particles is negligible (Wiedensohler, 1988). Considering both polarities, Eq. (2) therefore takes the following form

$$\frac{dN_{+1}}{dt} = n_i^+ \beta_0^+ N_0 - n_i^- \beta_{+1}^- N_{+1} \tag{3}$$

$$\frac{dN_{-1}}{dt} = n_i^- \beta_0^- N_0 - n_i^+ \beta_{-1}^+ N_{-1}. \tag{4}$$

The limiting-sphere theory divides the space surrounding a particle into two regions separated by an spherical boundary centered on the particle (Fuchs, 1963). In the inner region, extending from the particle surface to the limiting sphere, ion motion is governed by the ion's thermal speed and by the interaction potential between the ions and the particle. In the outer region, ion transport is described by macroscopic diffusion–mobility theory. The combination coefficient β of positive or negative ions with neutral or charged particles can be expressed as (Hoppel and Frick, 1986)

$$\beta = \frac{\pi \alpha \bar{c}_i \delta^2 \exp(-\phi(\delta)/k_B T)}{1+\exp(-\phi(\delta)/k_B T)\alpha \bar{c}_i \delta / 4 D_i \int_r^\infty 1/r^2 \exp(\phi(r)/k_B T)\, dr}. \tag{5}$$

Here, α is the probability that an ion entering the limiting sphere will collide with the particle and transfer its charge; $\bar{c}_i$ is the mean thermal speed of the ions; D_i is their diffusion coefficient; k_B is Boltzmann's constant; and T is the temperature; $\phi(r)$ is a function that describes the electrostatic potential between the particle and the ion at a radial distance r from the center of the particle, and δ is the limiting-sphere radius. The latter two are respectively given by:

$$\phi(r) = \frac{e^2}{4\pi\varepsilon}\left[\frac{i}{r} - \frac{{r_p}^3}{2r^2(r^2-{r_p}^2)}\right] \tag{6}$$

$$\delta = \frac{r_p}{Kn^2}\left[\frac{(1+(Kn))^5}{5} - \frac{(1+Kn^2)(1+(Kn^2))^3}{3} + \frac{2}{15}(1+(Kn^2))^{5/2}\right]. \tag{7}$$

https://doi.org/10.5194/ar-2026-29
Preprint. Discussion started: 4 August 2026

AEROSOL Research Discussions

In Eq. (6), ε is the dielectric constant, e is the elementary charge and i is integer number of elementary charges on the particle. In Eq. (7), Kn is the Knudsen number defined as $\mathrm{Kn} = \lambda_\mathrm{i}/r_\mathrm{p}$, where λ_i is the ion mean free path and r_p is the radius of the particle.

A numerical bipolar charging model applied in Nishida et al. (2025), based on the Hoppel and Frick (1986) charging model was used to solve the coupled system of ordinary differential equations (Eqs. 1 and 2).

In the free molecular regime ($r_\mathrm{p} \ll \lambda_\mathrm{i}$), which is close to the 20 nm size range, β primarily depends on thermal speed rather than a combination of thermal speed and electrical mobility. In this regime, the attachment coefficient can be described as (White, 1951)

$$\beta_{a\ll\lambda} = \pi {r_\mathrm{p}}^2 \bar{c}_\mathrm{i} \cdot \varepsilon^{-\frac{e^2}{r_\mathrm{p} k_\mathrm{B} T}}. \quad (8)$$

2.2 Inputs to theoretical model

The charging theory of Hoppel & Frick (1986) requires five ion properties to calculate the charging probabilities: electrical mobility, mass, diffusion coefficient, mean thermal speed and mean free path. Only two of these ion properties are independent: ion mobility and mass are used to derive the other three properties (Romay and Pui, 1992).

Given that the measurement of ion mass is nontrivial, experimental efforts were made to empirically relate ion mass to ion mobility. Among these, the empirical Kilpatrick (1971) mass-mobility relationship refined by Mäkelä et al. (1996) is amongst the most accepted one. This is given by:

$$Z_\mathrm{i} = \exp[-0.0347(\ln(m_\mathrm{i}))^2 - 0.0376\ln(m_\mathrm{i}) + 1.4662], \quad (9)$$

where Z_i is the ion electrical mobility and m_i is the ion mass. The mean free path of the ions is (Reischl et al., 1996)

$$\lambda_\mathrm{i} = \frac{16\sqrt{2}D_\mathrm{i}}{3\pi\bar{c}_\mathrm{i}}\left(\frac{m_\mathrm{g}}{m_\mathrm{g}+m_\mathrm{i}}\right)^{1/2}, \quad (10)$$

where m_g is the average mass of the neutral gas molecules. The ion diffusion coefficient is related to electrical mobility through the Einstein relation, $D_\mathrm{i} = (Z_\mathrm{i} k_\mathrm{B} T/e)$. The mean thermal speed, on the other hand, is related to mass through the kinetic theory of gases, $\bar{c}_\mathrm{i} = (8k_\mathrm{B}T/\pi m_\mathrm{i})^{1/2}$.

https://doi.org/10.5194/ar-2026-29
Preprint. Discussion started: 4 August 2026

AEROSOL Research Discussions

The weighted mean ion mobility $\langle Z_i \rangle$ of the measured distribution was used as input to the theoretical model, together with the weighted mean of the mean thermal speed $\langle \bar{c}_i \rangle$:

$$\langle Z_i \rangle = \frac{\sum_x n_{i,x} Z_{i,x}}{\sum_x n_{i,x}} \quad (11)$$

$$\langle \bar{c}_i \rangle = \frac{\sum_x n_{i,x} \bar{c}_{i,x}}{\sum_x n_{i,x}}, \quad (12)$$

where the summation is taken over all bins x. $\bar{c}_i$ was determined from the measured Z_i using the Kilpatrick (1971) mass-mobility relationship refined by Mäkelä et al. (1996) and the kinetic theory of gases. In the following sections, the weighted means $\langle Z_i \rangle$ and $\langle \bar{c}_i \rangle$ are referred to simply as the mean ion mobility and mean ion thermal speed, respectively.

The reason that the mean thermal ion speed was used as model input instead of the commonly used mean ion mass is that it more directly governs the charging dynamics in the sub-20 nm regime, reducing biases in the calculation of the combination coefficient, as explained in further detail in the Supplementary Information, Sect. S-1.

Other key model inputs include particle diameter (d_p) residence time in the charge conditioner (t), the initial average particle charge $\langle f \rangle_{t=0}$ and the ion production rate. Ion concentrations are solved using the following set of ODEs:

$$\frac{dn_i^+}{dt} = q_i^+ - \alpha_{rec} n_i^+ n_i^- - L_i^+ - \sum_q n_i^+ \beta_q^+ N_q \quad (13)$$

$$\frac{dn_i^-}{dt} = q_i^- - \alpha_{rec} n_i^+ n_i^- - L_i^- - \sum_q n_i^- \beta_q^- N_q, \quad (14)$$

where α_{rec} is a constant ion-ion recombination coefficient; L_i^+ and L_i^- are wall losses within the charge conditioner of positive and negative ions, respectively.

The magnitude of the initial average particle charge fraction $\langle f \rangle_{t=0}$ was set to +1 or −1, depending on the polarity of unipolar particles entering the charge conditioner; t is defined by the flow rate (3 L min^{-1}) and the charger volume (45 cm^3), which in our case was $t = V/Q$ = 0.9 s. Using typical ion generation rates of 10^8 ions cm^{-3}s^{-1} and $q_i^+ \approx q_i^-$, a steady-state charge distribution was reached (Adachi et al., 1985; Alonso and Alguacil, 2003; Clement and Harrison, 2000).

https://doi.org/10.5194/ar-2026-29
Preprint. Discussion started: 4 August 2026

2.3 Wiedensohler approximation

Despite the importance of ion properties in bipolar diffusion charging, reliably measuring these quantities alongside a mobility-based measurement is challenging in practice due to constraints of the instruments. Wiedensohler (1988) therefore proposed an approximation that has become a widely used practical solution for determining charge distributions needed for inverting electrical mobility spectrometer measurements. This approximation is based on a fit through the solutions obtained from the Fuchs (1963) model, including corrections on the α-parameters introduced by Hoppel & Frick (1986). Furthermore, the approximation assumes constant positive and negative ion mobilities of 1.35 and 1.60 $cm^2V^{-1}s^{-1}$, respectively (based on Bricard, 1949) as well as constant positive and negative ion masses of 140 and 101 Da, respectively, based on Hussin et al., 1983.

However, several studies have reported deviations in the measured charge fractions compared to this approximation (Chen and Jiang, 2018; De La Verpilliere et al., 2015; Jiang et al., 2014; Li et al., 2020, 2025; Nishida et al., 2025). A reason for these deviations includes variabilities in the ion properties, where the actual ion properties do not always correspond to the constant ion properties assumed in the approximation.

3 Methods

3.1 Experimental

Figure 1 illustrates the experimental setup used in our measurements. The setup, and its description in this section consists of the following stages described below: monodisperse particle generation, modification of the carrier gas composition, candidate charge conditioner, measurement of particle charge fractions, and measurement of charger ion electrical mobility.

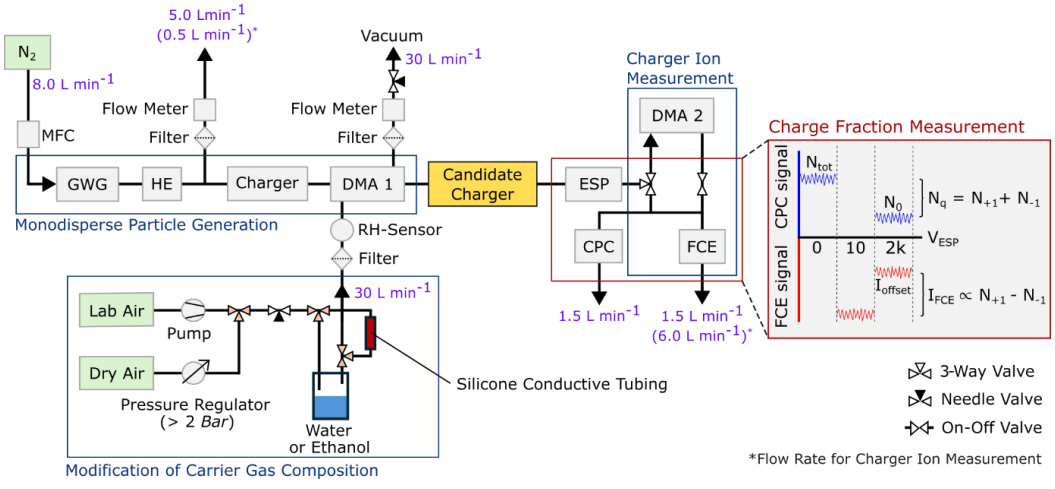

Figure 1: Schematic layout of the experimental setup to measure the particle charge fractions and the ion mobilities. Coloured valves are included to illustrate different configurations and are not present in the actual experimental setup. The graph illustrates the CPC and FCE signals for various ESP voltages, needed to determine the variables in Eq. (15). Key: MFC, mass flow controller; GWG: glowing wire generator; HE: heat exchanger

https://doi.org/10.5194/ar-2026-29
Preprint. Discussion started: 4 August 2026

215 **3.1.1 Monodisperse particle generation**

Tungsten-based nanoparticles were produced using a custom-built glowing wire generator employing a tungsten wire (0.4 mm diameter, 99.95 % purity, Advent Research Materials Ltd, Oxford, UK) and a quenching flow of 8 L min^{-1} nitrogen (Linde; 99.999 % purity). A gas-to-liquid heat exchanger set at 10°C was installed to limit the transfer of heat produced in the GWG through the metallic tubing towards downstream stages. Monodisperse particles of various sizes (3-20 nm) were
220 obtained by mobility classification using a Vienna-type Differential Mobility Analyzer (DMA 1) operated at an open-loop sheath flow rate (30 L min^{-1}) to control the composition of the carrier gas.

3.1.2 Modification of carrier gas composition

The gas composition downstream of DMA 1 was modified by changing the composition of the sheath gas. Specifically, VMS, water vapor or ethanol vapor were added to either laboratory air or dry air before passed as a sheath flow through
225 DMA 1.

VMS were added by passing the sheath flow through conductive silicone tubing (TSI Incorporated, Shoreview, MN, USA; length: 60 cm; inner diameter: 4.8 mm), which releases these compounds via outgassing. Aerosol particles passing through the candidate neutralizer were therefore exposed to VMS without passing through the silicone tubing. Assuming linear
230 scaling of the outgassing rate with tubing surface area and flow rate (Yu et al., 2009), a sheath flow rate of 30 L min^{-1} through this configuration yields VMS concentrations representative of the lower range typically encountered in aerosol measurements involving silicone tubing (i.e., flow rates < 5 L min^{-1}).

Constant concentrations of water or ethanol vapor were added by passing the sheath gas through a vessel containing liquid
235 water or ethanol. This yielded relative humidity (RH) levels of up to 45 % (1.4 vol %, 3×10^{17} water molecules cm^{-3}) or ethanol vapor concentrations of 1.5 vol % (4×10^{17} ethanol molecules cm^{-3}) at room temperature. The RH was measured using a RH-sensor (Vaisala Oyi, model HMP110), placed at the sheath flow inlet of the DMA. The ethanol vapor concentration, on the other hand, was estimated from the total consumption of liquid ethanol over the measurement period and the sheath flow rate.

240

Lab air was introduced using a diaphragm pump (KNF Neuberger GmbH, model N035.1.2AN.18), which inevitably outgasses species from previous uses or from heated components that change the air composition. In contrast, dry air was obtained from a HEPA filtered, compressed dry air supply. Although both sources consist nominally of air, their impurity compositions differ due to pump-related emissions and differences in processing and storage conditions.

245

https://doi.org/10.5194/ar-2026-29
Preprint. Discussion started: 4 August 2026

After changing the carrier gas composition, the system was flushed with the new gas mixture overnight before initiating a new measurement, as complete desorption of residual components from the inside tubing walls can require multiple hours (see Supplementary Information, Sect. S-2).

3.1.3 Candidate charge conditioner

The monodisperse particles exiting DMA 1 were passed at a flow rate of 3 L min^{-1} through two custom-built ^{63}Ni charge conditioners placed in-series. Each charge conditioner had the same geometry (rectangular, L×W×H = 10×3×1.5 cm) and an activity of 370 MBq. A critical point in the charge conditioning step is that it provides the aerosol particles with a steady-state charge distribution, because predictions of particle charge distributions are typically based on steady-state conditions. As we show in the Supplemental Information (Sect. S-3), a steady-state condition was reached only when using two charge conditioners in-series. The candidate charge conditioner was kept at a slight overpressure to avoid ambient air from entering the system through microscopic leaks. As will be shown in Sect. 4.1.1, trace amounts of compounds can, depending on their electron and proton affinity, significantly alter the charger ion composition and therefore affect the charger's performance.

3.1.4 Measurement of charge fractions

The measurement of the particle's charge fractions consisted of a custom-built electrostatic precipitator (ESP; see Supplementary Information, Sect. S-4), a Faraday Cup Electrometer (FCE; TSI 3068B) and an Ultrafine Condensation Nucleus Counter (CPC; TSI 3776). The CPC had a d_{50} of 2.7 nm, which denotes the particle diameter at which the 50 % of the particles are detected. The CPC and FCE were positioned in parallel with an equal tubing length from the upstream ESP and each was operated at a flow rate of 1.5 L min^{-1}, ensuring that the particle losses in the tubing to each of these instruments were the same.

The measurements of charge fractions were performed based on a similar methodology as described by Bello et al. (2024), where the underlying assumption is that sub-20 nm particles carry at most a single elementary charge q, i.e., $q = -1$, 0, or +1. The single charge follows from bipolar diffusion charging theory, which predicts that the probability of multiple charging is negligible in this size range (Fuchs, 1963; Wiedensohler, 1988).

For all the monodisperse particle samples downstream of DMA 1, the voltage across the ESP was stepped consecutively at 0 V, 10 V, 2 kV and 0 V at 1-minute intervals. The resulting CPC and FCE measurements then yielded the variables needed to determine the fraction of singly charged particles (see Fig. 1) as follows:

$$f_{\pm 1} = \frac{N_{\mathrm{q}\pm}\, C \cdot I_{\mathrm{FCE}}/Qe}{2N_{\mathrm{tot}}}, \tag{15}$$

https://doi.org/10.5194/ar-2026-29
Preprint. Discussion started: 4 August 2026

where N_q is the concentration of charged particles, which is the difference between the total particle concentration (N_{tot}; measured by the CPC when the ESP was operated at 0 V) and the neutral particle concentration (N_0; measured by the CPC when the ESP was operated at 2 kV); I_{FCE} is the current measured by the FCE while the ESP is operated at 10 V; Q is the volumetric flow rate through the FCE; e is the electron charge and C is a correction factor that accounts for particle losses due to operating the ESP at 10 V (see Supplementary Information, Sect. S-5).

The ESP was operated at 10 V during the I_{FCE} measurement to remove ions generated by the candidate charge conditioner. This ensures that these ions are electrostatically precipitated, thereby preventing them from contributing to the measured particle signal in the FCE.

A second measurement with the ESP operated at 0 V was performed at the end of each series to record any systematic changes in particle production rate in the GWG throughout the 4-minute measurement period per particle diameter. In addition, operating the ESP at 2 kV served not only to determine N_0 from the CPC recording but also to repeatedly assess the offset of the FCE.

3.1.5 Measurement of charger ions

Before and after the measurement of particle charge fractions, the electrical mobility of the ions produced in the candidate charge conditioner was measured by switching the two valves in the measurement stage (see Fig. 1), thereby directing the flow through the half-mini DMA (DMA 2) for electrical mobility classification (Fernandez De La Mora, 2017). The flow rate through the FCE was increased to 6 L min^{-1} to minimize ion diffusion losses during transport from the candidate charger to the FCE.

DMA 2 was operated at a closed-loop sheath flow of 300 L min^{-1} and a resolution of 10 at full width at half maximum (FWHM), which was determined by calibration with the tetraheptylammonium bromide monomer (THAB; 0.97 $cm^2V^{-1}s^{-1}$). The measured mobility-resolved ion concentrations were subsequently corrected for transmission losses within the DMA, using the relation between penetration and particle diameter (d_p) given by Cai et al. (2018), as shown in the Supplementary Information, Sect. S-6.

4 Results and discussion

In the following sections, the effects on the charge distribution of using conductive silicone tubing (Sect. 4.1), relative humidity (Sect. 4.2), and adding ethanol vapor (Sect. 4.3) are discussed.

https://doi.org/10.5194/ar-2026-29
Preprint. Discussion started: 4 August 2026

The measured charge fractions are compared with those predicted by the numerical model based on Hoppel & Frick (1990), as well as the charge fractions obtained from the Wiedensohler (1988) approximation. All relative differences of the model and approximation are defined with respect to the measurement, i.e.

$$\Delta_{\mathrm{rel}}(\%) = \left(\frac{f_{\mathrm{p}} - f_{\mathrm{m}}}{f_{\mathrm{m}}}\right) \cdot 100\ \%, \tag{16}$$

where f_{m} is the measured charge fraction and f_{p} is the charge fraction predicted by either the model or the Wiedensohler (1988) approximation. Moreover, the mean relative differences are determined over the size ranges 6-20 nm, omitting smaller particles for which the uncertainty in the measured charge fractions is high due to significant particle losses.

4.1 Addition of VMS

In the results presented below, volatile methyl siloxanes were introduced into the carrier gas using conductive silicone tubing, which releases these compounds via outgassing.

4.1.1 Ion mobility distributions

Figure 2 shows the electrical mobility distributions of positive and negative ions, along with their concentration-weighted mean, produced when dry air was passed through the candidate charger with and without the use of silicone tubing. The generated ions of both polarities exhibit electrical mobilities ranging from 0.8 to 2.6 $\mathrm{cm^2V^{-1}s^{-1}}$, corresponding to approximate molecular masses between 28 Da and 637 Da (Mäkelä et al., 1996).

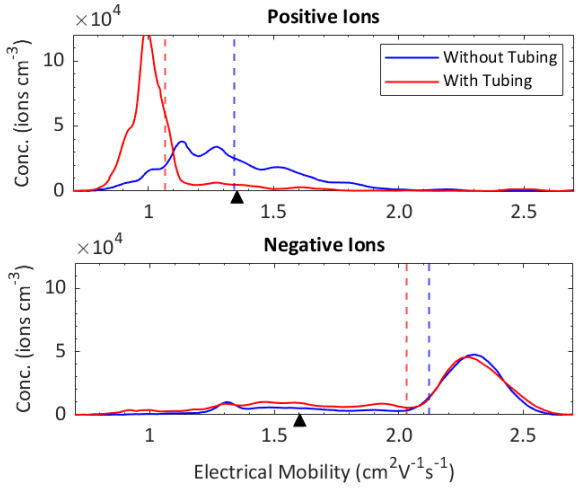

Figure 2: Mobility distributions of positive and negative ions produced in dry air and the ^{63}Ni radioactive source with and without the use of silicone tubing upstream the charger. The vertical dashed lines indicate the weighted mean of the distribution of the respective colour, and the triangles show the electrical mobility values used in the Wiedensohler (1988) approximation.

https://doi.org/10.5194/ar-2026-29
Preprint. Discussion started: 4 August 2026

When ionizing dry air without using conductive silicone tubing, the mean negative electrical mobility $\langle Z_i^- \rangle$ is 2.12 $cm^2V^{-1}s^{-1}$, where the mobility spectrum of the negative ions is dominated by species with mobilities near 2.30 $cm^2V^{-1}s^{-1}$ corresponding to masses around 43 Da (Mäkelä et al., 1996), primarily attributed to small, highly mobile species such as nitrite and nitrate (NO_2^-; 46 Da or NO_3^-; 62 Da; Schmidt-Ott et al., 2024; Steiner et al., 2014), which are formed within the ionization source from N_2 and O_2. Owing to their high electron affinity, these ions tend to dominate the negative ion population, thereby suppressing the negative ionization of compounds with lower electron affinity. As a result, species with lower electron affinity remain either neutral or become positively charged.

The broad range of the positive ion mobility spectrum, having a mean mobility $\langle Z_i^+ \rangle$ of 1.34 $cm^2V^{-1}s^{-1}$, shows exactly this phenomenon, where most species in the gas have an electron affinity lower than that of the most electronegative species and thus become positively charged. Most of those species ending up with a positive charge are organic compounds, that generally also have high proton affinity forming protonated organic molecules (Maißer et al., 2015).

When placing silicone tubing upstream of the charge conditioner, $\langle Z_i^+ \rangle$ decreased by 20 % to 1.07 $cm^2\,V^{-1}\,s^{-1}$, which can be attributed to trace concentrations of VMS outgassing from the tubing that have a low electron affinity and high proton affinity, and hence take up most positive charges, leaving other compounds largely uncharged (Schmidt-Ott et al., 2024). With the mobility data it is not possible to determine the exact chemical composition, but the peak mobility of the positive ions of 0.99 $cm^2\,V^{-1}\,s^{-1}$ likely corresponds to the electrical mobility of the D6, D7 or D8 VMS oligomer (Kilpatrick, 1971; Li et al., 2025; Maißer et al., 2015).

Given that nearly all positive charges created in the charge conditioner attach to or are transferred to a neutral VMS (see Fig. 2), the concentration of neutral VMS outgassing from the silicone tubing is necessarily at least the concentration of the positive charges produced inside the charger of ~10^6 – 10^9 ions cm^{-3}, corresponding to ~0.04 – 40 ppt (Adachi et al., 1993; Biskos et al., 2005; Chen et al., 2024; Kimoto et al., 2011). These orders of magnitude of neutral VMS concentration is consistent with measurements by Yu et al. (2009), who reported concentrations in the ppt-range outgassing from conductive silicone tubing. These findings demonstrate that trace gases can, depending on their electron and proton affinity, significantly modify the charger ion composition and therefore the charger's performance.

On the other hand, the mean negative ion mobility was largely unaffected by the addition of VMS, changing by only 4 % compared to the case without VMS to $\langle Z_i^- \rangle$ = 2.03 $cm^2\,V^{-1}\,s^{-1}$. This finding is consistent with previous measurements, which showed that VMS affected only the positive ion mobility spectrum (Schmidt-Ott et al., 2024).

https://doi.org/10.5194/ar-2026-29
Preprint. Discussion started: 4 August 2026

4.1.2 Particle charge fractions

Figure 3 shows the measured sub-20 nm fractions of singly charged particles of both positive and negative polarity, with and without employing silicone tubing in the experimental setup, together with the respective modelled and approximated (Wiedensohler, 1988) charge fractions. The charge fractions were modelled using the measured mean ion properties (see Fig. 2) as model input. Note that the increase in charge fraction at low particle dimeters are systematic outliers, which are difficult to avoid at this size range due to the high particle losses.

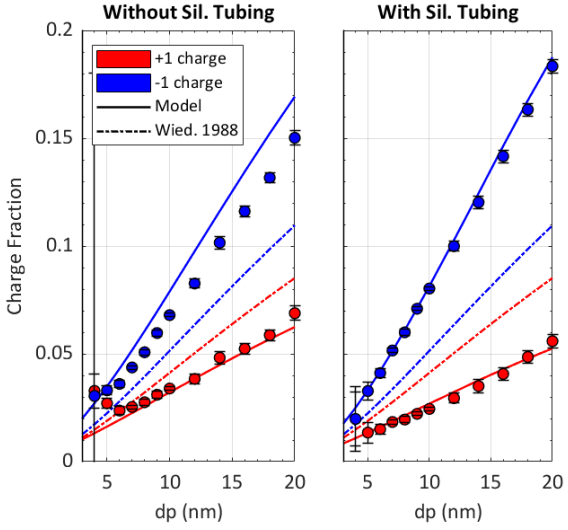

Figure 3: Measured and predicted fractions of singly charged particles of positive and negative polarity, without and with conductive silicone tubing installed upstream the charge conditioner. Predicted fractions were obtained from the Wiedensohler approximation and the theoretical model, the latter using the measured mean ion properties (Fig. 2) as input.

When silicone tubing is used, the model and measurement agree well, with relative differences of −6.1% and 0.6 % for positive and negative charge fractions, respectively. In contrast, without using silicone tubing, the agreement between the model and the measurement worsened, with relative differences of 4.2 % and 17.8 % for positive and negative charge fractions, respectively.

The poorer agreement when omitting silicone tubing likely arises from an inevitable artefact in the measurement of the mean ion mobility used as model input, caused by changes in the ion composition downstream the charge conditioner. As discussed in more detail the Supplemental Information (Sect. S-7), the weighted mean mobility changes as a function of the travelling distance from the charge conditioner to the DMA. As a result, the mobility measured by the DMA does not accurately represent the ion population inside the charge conditioner, introducing biases in the modelled particle charge

https://doi.org/10.5194/ar-2026-29
Preprint. Discussion started: 4 August 2026

fractions. This artefact strongly reduces when the ion mobility distribution is narrow, as is the case when silicone conductive tubing is employed upstream the charge conditioner (see Fig. 2).

The relative difference between the measurement and the Wiedensohler (1988) approximation is 35.7 % and −23.5 % for positive and negative charge fractions, respectively, as silicone tubing is omitted. When adding silicone tubing, the difference between measurement and approximation increases to 65.1 % and −38.1 % for positive and negative charge fractions, respectively.

Given the excellent agreement with the Hoppel & Frick-based model when silicone tubing is used, the discrepancies between the measured charge fractions and those predicted by the Wiedensohler (1988) approximation can be primarily attributed to differences in the underlying assumptions of these two methods to predict the charge fractions: in the Wiedensohler approximation, fixed ion properties are assumed, whereas in the model based on the Hoppel & Frick theory, ion properties correspond to the actual ion properties.

Furthermore, the relative difference in measured particle charge fraction between the cases when the conductive silicone tubing was used or not in the experiments is −24.6 % and +20.2 % for the positive and negative polarity, respectively. These changes in charge fraction are directly linked to the decrease in the mean positive ion mobility caused by the addition of VMS (see Fig. 2): the decreased electrical mobility of the positive ions decreases their collision frequency with both neutral particles (reduced +1 charging) and negatively charged particles (reduced neutralization). Consequently, the fraction of positively charged particles decreases, while the fraction of negatively charged particles increases.

4.2 Effect of relative humidity

In the measurements shown in the following section, the relative humidity in the carrier gas was changed by adding water vapor to the sheath flow of the DMA.

4.2.1 Ion mobility distributions

Figure 4 shows the positive and negative ion mobility distributions at varying humidity levels when using or omitting silicone tubing. It shows that the electrical mobility of the charger ions decreases as humidity levels increase, which can be explained by ion growth. This growth can be attributed to the clustering of the ions with water molecules, where hydrogen bonds facilitate the formation of larger ion-molecule clusters (Hyttinen et al., 2018). The decrease in ion electrical mobility with increasing relative humidity aligns with previous studies, that observed significant ion growth with increasing humidity (Li et al., 2025; Liu et al., 2020).

https://doi.org/10.5194/ar-2026-29
Preprint. Discussion started: 4 August 2026

Figure 4 also shows that when silicone tubing is employed, the mean positive ion electrical mobility remains relatively stable across varying humidity levels, near values associated with VMS, where $\langle Z_i^+ \rangle$ decreases by only 1.8 % as RH increases from 0 to 40 %. In contrast, when silicone tubing is removed, the positive ions show significantly stronger growth, with $\langle Z_i^+ \rangle$ decreasing by 12.7 %.

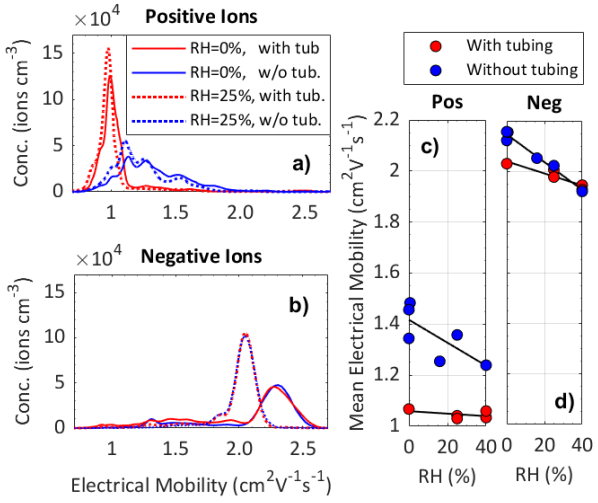

Figure 4: Mobility distributions of positive (a) and negative (b) ions generated at varying humidity levels when using or omitting silicone tubing upstream of the ionizer, together with the corresponding mean electrical mobilities (c and d).

Furthermore, without using silicone tubing, positive ions exhibit relatively large variability (scatter) in mean electrical mobility with increasing humidity (Fig. 4c), whereas this variability is significantly smaller for the negative ions (Fig. 4d). One possible explanation is that clustering with water molecules is more complex for the positive polarity, because the ion population comprises multiple species, each interacting differently with water molecules. In contrast, the negative ion population is dominated by only a few species, such as NO_2^- and NO_3^-, leading to a more systematic growth with increasing humidity.

4.2.2 Particle charge fractions

Figure 5 shows the measured charge fractions of positively and negatively charged particles for varying humidity levels when employing silicone tubing, together with the modelled charge fractions based on the measured ion properties. The figure shows that there is a good agreement between the measured data and the Hoppel & Frick prediction. Increasing the RH from 0 to 40 % leads to a decrease in the negative charge fraction of 10 nm particles by 8.9 % (measured) and 9.7 % (modelled), while the positive charge fraction increases by 0.1 % (measured) and 3.0 % (modelled).

https://doi.org/10.5194/ar-2026-29
Preprint. Discussion started: 4 August 2026

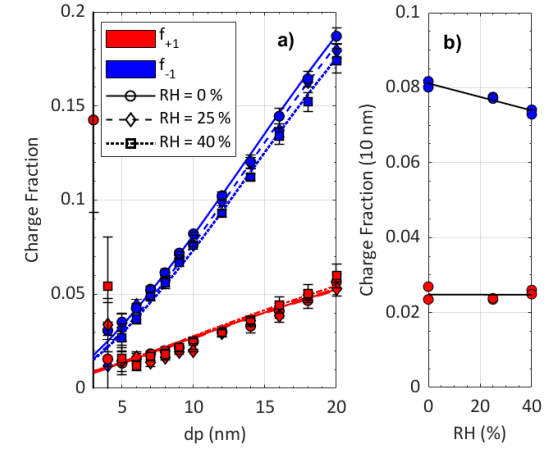

Figure 5: Measured and modelled charge fractions of positively and negatively charged particles at varying relative humidity using silicone tubing upstream of the ionizer: (a) size-dependent charge fractions for sub-20 nm particles, and (b) measured charge fractions for 10 nm particles. The measured mean ion properties used as model inputs are shown in Fig. 4.

On the other hand, Fig. 6 shows that when silicone tubing is omitted, there is a poorer agreement between the measurement and model, for the same reasons stated in Sect. 4.1.2. Fig. 6b shows that the measured charge fractions of both positive and negative particles are more scattered when the silicone tubing is omitted, compared to the case when silicone tubing is used. This behavior is consistent with the ion electrical mobility measurements, where the positive ion mobility is more variable with changes in humidity levels when the tubing is omitted, which directly affects the charging behavior. Overall, increasing the RH from 0 to 40 % leads to a decrease in the negative charge fraction of 10 nm particles by 5.5 % (measured) and 13.2 % (modelled), while the positive charge fraction increases by 3.0 % (measured) and 3.3 % (modelled).

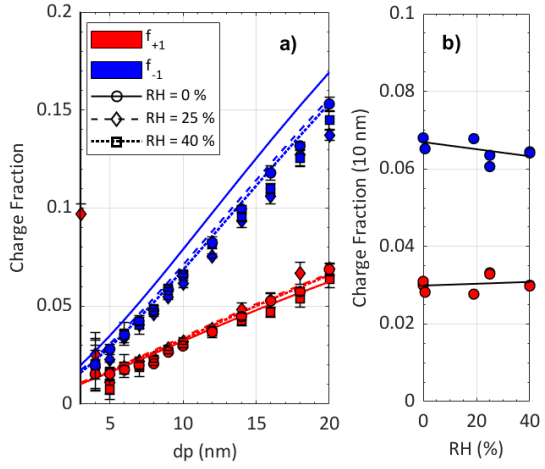

Figure 6: Measured and modelled charge fractions of positively and negatively charged particles at varying relative humidity without silicone tubing upstream of the ionizer: (a) size-dependent charge fractions for sub-20 nm particles, and (b) measured charge fractions for 10 nm particles. The measured mean ion properties used as model inputs are shown in Fig. 4.

https://doi.org/10.5194/ar-2026-29
Preprint. Discussion started: 4 August 2026

AEROSOL Research Discussions

4.3 Addition of ethanol vapor

In a final series of measurements, ethanol vapor was added to the carrier gas to produce ions with different properties than those discussed above, and consequently different charging dynamics compared to the two cases presented in Sect. 4.1 and 4.2.

4.3.1 Ion mobility distributions

Figure 7 shows the ion mobility distributions with and without the addition of ethanol vapor. When adding ethanol vapor, $\langle Z_i^+ \rangle$ decreased by only 3.0 % (from 1.34 to 1.30 $cm^2V^{-1}s^{-1}$), whereas $\langle Z_i^- \rangle$ decreased significantly by 27.8 % (from 2.12 to 1.53 $cm^2V^{-1}s^{-1}$). The low-mobility species likely correspond to large ethanol-containing cluster ions (Kohno et al., 1999).

The electrical mobility of both positive and negative ions strongly depends on the concentration of added ethanol. As the vapor concentration increases, the mean mobilities of positive and negative ions decrease and gradually converge to similar values. Similar observations were reported by Mäkelä et al. (1996) for acetone vapor, who attributed this effect to ion growth through ion-induced nucleation.

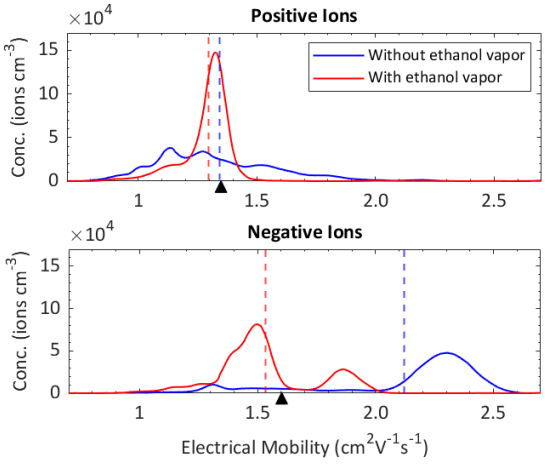

Figure 7: Mobility distributions of positive and negative ions produced by the ^{63}Ni radioactive source with and without adding ethanol vapor to the carrier gas. The vertical striped lines indicate the weighted mean of the distribution of the respective colour, and the triangles show the electrical mobility values used in the Wiedensohler (1988) approximation.

https://doi.org/10.5194/ar-2026-29
Preprint. Discussion started: 4 August 2026

4.3.2 Particle charge fractions

Figure 8 shows that upon addition of ethanol vapor, the negative charge fraction decreases while the positive charge fraction increases. This is consistent with the measured changes in ion properties, where the strong decrease in negative ion mobility shifts the charge balance toward positive charging, thereby increasing the positive charge fraction and reducing the negative charge fraction. Moreover, the measured charge fractions are in good agreement with the model predictions, deviating by only 2.0 % for the positive and 8.2 % for the negative charge fraction.

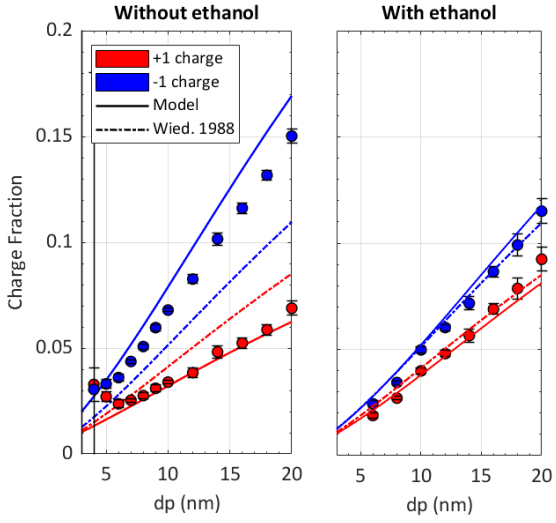

Figure 8: Measured and predicted fractions of singly charged particles of positive and negative polarity, without and with adding ethanol vapor to the carrier gas. Predicted fractions were obtained from the Wiedensohler approximation and the theoretical model, the latter using the measured ion properties (Fig. 7) as input.

The relatively good agreement between the Hoppel & Frick model and measurement when ethanol vapor is added, compared with the non-ethanol case, can be explained by a similar reasoning as discussed in Sect. 4.1.2: a narrower distribution of ion properties results in a more accurate measurement of ion properties that are used as model input, and thus yields more accurate model predictions. Furthermore, a narrow distribution of ion properties minimizes averaging errors relating to the calculation of the combination coefficient β.

Interestingly, the charge fractions from the Wiedensohler (1988) approximation show relatively good agreement once ethanol is added, differing from the measurements by only 4.6 % and 5.0 % for positive and negative charge fractions, respectively. This improved agreement can be attributed to the similarity between the electrical mobility of the ions assumed in the approximation and those measured in the used ethanol conditions. Specifically, the measured positive and negative ion electrical mobilities differ from those used in the approximation by only −3.7 % and −4.4 %, respectively.

https://doi.org/10.5194/ar-2026-29
Preprint. Discussion started: 4 August 2026

AEROSOL Research Discussions

5 Approximation of ion properties

In the previous sections, we experimentally demonstrated that the steady-state particle charge distribution is primarily governed by charger ion properties, which can be predicted from Hoppel & Frick theory. We also showed that these ion properties can be strongly influenced by trace gases present in the sampled air, making the particle charge state sensitive to the sampling environment.

Figure 9 summarizes the electrical mobilities of positive and negative ions reported in various studies together with those measured in the current study (Schmidt-Ott et al., 2024; Tigges et al., 2015). It shows that there exist significant variabilities in ion properties between different measurements, with Z_i^+ ranging from 1.0 to 2.0 $cm^2V^{-1}s^{-1}$ and Z_i^- from 1.1 to 2.5 $cm^2V^{-1}s^{-1}$. The figure also shows that in all cases that a silicon-based tubing is employed, Z_i^+ is confined within a very narrow range (i.e., 1.05 ± 0.10 $cm^2V^{-1}s^{-1}$; see Sect. 4.1). In contrast, the negative ion properties remain highly variable and depend on the composition of the air (see Sect. 4.2).

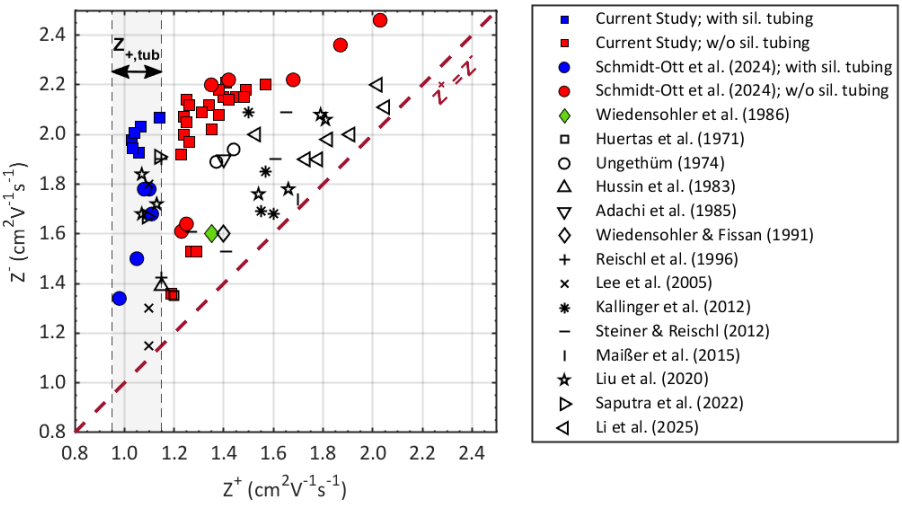

Figure 9: Mean electrical mobility of positive and negative ions reported in previous studies conducted under a variety of air compositions and charging techniques. The data in the figure is based on historical ion mobility values summarized by Tigges et al. (2015) and supplemented with values reported in more recent studies.

Based on the controllable positive ion properties when silicone tubing is employed, we here present a method to experimentally derive the negative ion properties. Altogether, knowledge of both ion properties enables us to predict the charge fractions by applying the Hoppel–Frick theory.

https://doi.org/10.5194/ar-2026-29
Preprint. Discussion started: 4 August 2026

For particles in the continuum ($r_p \approx \lambda_i$) and transitional ($r_p \gg \lambda_i$) regime, the ratio of positive to negative charge fractions can be expressed as a function of ion electrical mobility (Chen and Jiang, 2018; Nishida et al., 2020).

$$f_{+1}/f_{-1} = (Z_i^+/Z_i^-)^{2q}, \quad (17)$$

where q is the number of elementary charges carried by the particles. This relation follows from a simplified version of the Fuchs model by Gunn-Woessner equation, where the charge fraction depends solely on the electrical mobility ratio, rather than on the thermal speed.

However, in the free-molecular limit ($r_p \ll \lambda_i$), particle charging is governed primarily by thermal (ballistic) ion transport rather than diffusive transport. In this regime, the charging rate therefore depends explicitly on the mean thermal speed of the ions, and electrical mobility no longer appears in the definition of the combination coefficient (see Eq. 8).

Consequently, a relation between the charge fractions and the mean thermal ion speed can be derived from the Hoppel–Frick theory for 20 nm particles, as demonstrated in the Supplementary Information (Sect. S-11), which is

$$(f_{+1}/f_{-1})_{20\mathrm{nm}} = (c_i^+/c_i^-)^{\alpha}, \quad (18)$$

where α = 1.591. Furthermore, by definition,

$$(f_{+1}/f_{-1})_{20\mathrm{nm}} = (N_{+1}/N_{-1})_{20\mathrm{nm}}, \quad (19)$$

where N_{+1}/N_{-1} denotes the ratio of positively to negatively singly charged particle concentrations. For particles with a diameter of 20 nm, this ratio can be readily determined through bipolar MPSS measurement, because multiple charging is negligible at this size and thus mobility-classified particles correspond to a single diameter (Wiedensohler, 1988).

As we have seen, the positive ion properties are well-defined when employing conductive silicone tubing, and Z_i is closely linked to c_i through the empirical mass-mobility relation and kinetic theory (Sect. 2.2). By equating Eq. (18) and Eq. (19) it is therefore possible to determine the negative ion properties, as illustrated in Fig. 10. Knowledge of the positive ion properties and the approximated negative ion properties then allows to derive the particle charge fractions f_q^+ and f_q^- for all particle diameters and charge states q using Hoppel & Frick (1986) theory.

https://doi.org/10.5194/ar-2026-29
Preprint. Discussion started: 4 August 2026

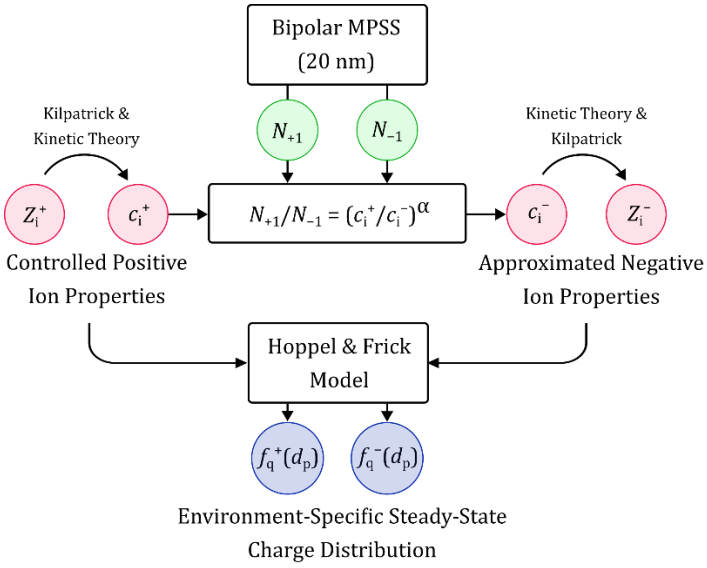

Figure 10: Schematic of the method to determine the local bipolar charge distribution through an approximation of the negative ion properties.

The uncertainty in the determined f_q^+ and f_q^- is governed by uncertainty in the assumed value of Z_i^+; measurement uncertainty in $(N_{+1}/N_{-1})_{20nm}$ and uncertainty related to the usage of the empirical Kilpatrick mass-mobility relation. We have shown in this work that the usage of the Kilpatrick (1971) mass-mobility relationship refined by Mäkelä et al. (1996) yields fairly accurate results. Furthermore, random errors in determining N_{+1}/N_{-1} through bipolar MPSS can be kept relatively small through long averaging times, and any systematic errors cancel in the ratio.

Figure 11 shows the modelled particle charge distribution using the method shown in Fig. 10, compared to the measured charge distribution of sub-20 nm particles. Since we do not have a direct measurement of N_{+1} and N_{-1} for the term $(N_{+1}/N_{-1})_{20nm}$, we used the measured $(f_{+1}/f_{-1})_{20nm}$ instead, as the two quantities are equivalent. The measured and approximated charge fractions agree within 5.4 % and 4.7 % for positive and negative polarity, respectively.

https://doi.org/10.5194/ar-2026-29
Preprint. Discussion started: 4 August 2026

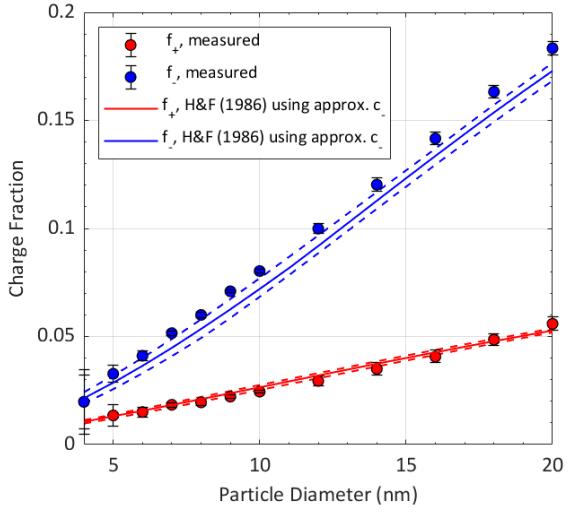

Figure 11: Measured and modelled steady-state charge fractions for sub-20 nm particles. The modelled distribution is determined from the approximated negative ion properties (c_i^- = 279 ms^{-1} and Z_i^- = 1.89 cm^{2}V^{-1}s^{-1}) and the controlled positive ion properties, using a measured ratio $(N_{+1}/N_{-1})_{20nm}$ = 0.304 as input. The dotted lines represent the error margins that arise from the propagated error of the assumed Z_i^+ (1.05 ± 0.10 cm^{2}V^{-1}s^{-1}), which propagates both through the approximation of c_i^- and through the model.

6 Conclusions

In this work, we show that measured charge fractions show excellent agreement with charge fractions predicted by Hoppel & Frick theory, with relative differences of up to −6.1 % and 0.6 % for positive and negative charge fractions, respectively, provided that the underlying ion properties are accurately measured. These results support the validity of classical charging theory for sub-20 nm particles.

On the other hand, discrepancies exist between the measured charge fractions and those predicted by the widely used Wiedensohler (1988) approximation, reaching 35.7 % and −23.5 % for positive and negative charge fractions, respectively, with the discrepancies nearly doubling when conductive silicone tubing is employed.

By varying the charger ion properties while measuring the particle charge fractions, we experimentally demonstrate that charger ion properties are the dominant factor governing the particle charge distribution. We demonstrate that trace concentrations of volatile methyl siloxanes (VMS) outgassed from conductive silicone tubing significantly affect ion properties, changing the measured charge fractions by up to 25 % compared with the case in which the tubing is omitted. This finding highlights the importance of trace gases in aerosol charging. Our results also show that, for relative humidity

https://doi.org/10.5194/ar-2026-29
Preprint. Discussion started: 4 August 2026

levels up to 40 %, the uncertainty in the measured charge fractions remained below 10 % for the gas compositions encountered during this study.

The influence of trace gases provides a further explanation for the large variability in ion properties reported across different studies over the past decades. These variations directly translate into variabilities in bipolar aerosol charging across different sampling environments, for which current MPSS inversion methods based on fixed ion properties cannot account.

Furthermore, we show that positive ion properties can be readily stabilized within a narrow range of repeatable values at varying gas compositions by using silicone conductive tubing upstream the charge conditioner. Negative ion properties, on the other hand, remain dependent on the gas composition and in particular on relative humidity. Further research is needed to control the negative ion properties too, possibly by adding dopants of known composition with a high electron affinity.

Building on the finding that positive ion properties can to some extent be controlled, we show that negative ion properties can be approximated through a simple bipolar MPSS measurement when silicone-based conductive tubing is employed. Together, the controlled positive and approximated negative ion properties provide a more complete ion property input required for Hoppel & Frick theory to predict the environment-specific particle charge distribution.

Lastly, we also show that several conventional bipolar chargers did not produce a steady-state charge distribution on sub-20 nm particles. Establishing a steady-state charge distribution on the sampled aerosol is essential for predicting particle charge distributions. However, in routine MPSS measurements, it is generally difficult to verify whether steady-state conditions have been achieved. Further research is therefore needed to develop simple methods for verifying that steady-state conditions are achieved in conventional MPSS measurements.

https://doi.org/10.5194/ar-2026-29
Preprint. Discussion started: 4 August 2026

Code and data availability

A link to the data will be provided.

Supplement link

The link to the supplement will be included by Copernicus, if applicable.

Author contributions

F. Schmidt-Ott carried out all experiments, performed the data analysis, and prepared the original draft of the manuscript. R. Nishida developed the main theoretical model, made significant contributions on advising on the experimental measurements, and contributed to manuscript revision. S. Schmitt provided valuable contribution to the development of the measurements concepts and contributed to manuscript revision. J. Olfert contributed to the conception the primary measurement method and contributed to manuscript revision. G. Biskos significantly contributed to the development of new research ideas and contributed to manuscript revision. J. Kangasluoma supervised the research, advised on the experimental measurements and contributed to manuscript revision.

Competing interests

At least one of the (co-)authors is a member of the editorial board of Aerosol Research.

Disclaimer

Publisher's note: “Copernicus Publications remains neutral with regard to jurisdictional claims made in the text, published maps, institutional affiliations, or any other geographical representation in this paper. While Copernicus Publications makes every effort to include appropriate place names, the final responsibility lies with the authors. Views expressed in the text are those of the authors and do not necessarily reflect the views of the publisher.”

Acknowledgements

We gratefully thank the technical staff of INAR, Pekka Rantela, Hannu Koskenvaara, Pasi Aalto, Jarkko Mäntylä, Antti Lohti, Tommy Chan and Petri Keronen, for their invaluable support during the experimental work. The authors acknowledge the use of ChatGPT (OpenAI) for language editing and improvement of the manuscript text.

Financial support

This research has been supported by the Research council of Finland (projects 356134, 364223, 325656)

https://doi.org/10.5194/ar-2026-29
Preprint. Discussion started: 4 August 2026

References

Adachi, M., Kousaka, Y., and Okuyama, K.: Unipolar and bipolar diffusion charging of ultrafine aerosol particles, Journal of Aerosol Science, 16, 109–123, https://doi.org/10.1016/0021-8502(85)90079-5, 1985.

Adachi, M., Okuyama, K., Kozuru, H., Kousaka, Y., and Pui, D. Y. H.: Bipolar Diffusion Charging of Aerosol Particles Under High Particle/Ion Concentration Ratios, Aerosol Science and Technology, 11, 144–156, https://doi.org/10.1080/02786828908959307, 1989.

Adachi, M., Pui, D. Y. H., and Liu, B. Y. H.: Aerosol Charge Neutralization by a Corona Ionizer, Aerosol Science and Technology, 18, 48–58, https://doi.org/10.1080/02786829308959583, 1993.

Alonso, M. and Alguacil, F. J.: The effect of ion and particle losses in a diffusion charger on reaching a stationary charge distribution, Journal of Aerosol Science, 34, 1647–1664, https://doi.org/10.1016/S0021-8502(03)00357-4, 2003.

Asbach, C., Kaminski, H., Lamboy, Y., Schneiderwind, U., Fierz, M., and Todea, A. M.: Silicone sampling tubes can cause drastic artifacts in measurements with aerosol instrumentation based on unipolar diffusion charging, Aerosol Science and Technology, 50, 1375–1384, https://doi.org/10.1080/02786826.2016.1241858, 2016.

Bello, O. W., Kazemimanesh, M., Kostiuk, L., and Olfert, J. S.: The effect of sodium chloride on the charge state of soot particles in a laminar diffusion flame, Combustion and Flame, 269, 113691, https://doi.org/10.1016/j.combustflame.2024.113691, 2024.

Biskos, G., Reavell, K., and Collings, N.: Electrostatic characterisation of corona-wire aerosol chargers, Journal of Electrostatics, 63, 69–82, https://doi.org/10.1016/j.elstat.2004.07.001, 2005.

Bricard, P. J.: L'Equlibre ionique De La basse atmosphere, J. Geophys. Res., 54, 39–52, https://doi.org/10.1029/JZ054i001p00039, 1949.

Cai, R., Attui M., Jiang, J., Korhonen, F., Hao, J., Petäjä, T., and Kangasluoma, J.: Characterization of a high-resolution supercritical differential mobility analyzer at reduced flow rates, Aerosol Science and Technology, 52, 1332–1343, https://doi.org/10.1080/02786826.2018.1520964, 2018.

Chen, X. and Jiang, J.: Retrieving the ion mobility ratio and aerosol charge fractions for a neutralizer in real-world applications, Aerosol Science and Technology, 52, 1145–1155, https://doi.org/10.1080/02786826.2018.1498587, 2018.

Chen, X., Zhou, F., Zhang, Q., Jiang, F., Jiang, J., and Zhang, Z.: A low-cost and miniature aerosol charger using americium-241, Aerosol Science and Technology, 58, 957–964, https://doi.org/10.1080/02786826.2024.2359558, 2024.

Clement, C. F. and Harrison, R. G.: Enhanced localised charging of radioactive aerosols, Journal of Aerosol Science, 31, 363–378, https://doi.org/10.1016/S0021-8502(99)00064-6, 2000.

De La Verpilliere, J. L., Swanson, J. J., and Boies, A. M.: Unsteady bipolar diffusion charging in aerosol neutralisers: A non-dimensional approach to predict charge distribution equilibrium behaviour, Journal of Aerosol Science, 86, 55–68, https://doi.org/10.1016/j.jaerosci.2015.03.006, 2015.

Fernandez De La Mora, J.: Expanded flow rate range of high-resolution nanoDMAs via improved sample flow injection at the aerosol inlet slit, Journal of Aerosol Science, 113, 265–275, https://doi.org/10.1016/j.jaerosci.2017.07.020, 2017.

Fuchs, N. A.: On the stationary charge distribution on aerosol particles in a bipolar ionic atmosphere, Geofisica Pura e Applicata, 56, 185–193, https://doi.org/10.1007/BF01993343, 1963.

Gopalakrishnan, R., McMurry, P. H., and Hogan, C. J.: The Bipolar Diffusion Charging of Nanoparticles: A Review and Development of Approaches for Non-Spherical Particles, Aerosol Science and Technology, 49, 1181–1194, https://doi.org/10.1080/02786826.2015.1109053, 2015.

Hinds, W. C.: Aerosol Technology: Properties, Behavior, and Measurement of Airborne Particles, Wiley, 1999.

Hoppel, W. A. and Frick, G. M.: Ion—Aerosol Attachment Coefficients and the Steady-State Charge Distribution on Aerosols in a Bipolar Ion Environment, Aerosol Science and Technology, 5, 1–21, https://doi.org/10.1080/02786828608959073, 1986.

https://doi.org/10.5194/ar-2026-29
Preprint. Discussion started: 4 August 2026

Hoppel, W. A. and Frick, G. M.: The Nonequilibrium Character of the Aerosol Charge Distributions Produced by Neutralizers, Aerosol Science and Technology, 12, 471–496, https://doi.org/10.1080/02786829008959363, 1990.

Huertas, M. L., Marty, A. M., Fontan, J., Alet, I., and Duffa, G.: Measurement of mobility and mass of atmospheric ions, Journal of Aerosol Science, 2, 145–150, https://doi.org/10.1016/0021-8502(71)90021-8, 1971.

Hussin, A., Scheibel, H. G., Becker, K. H., and Porstendörfer, J.: Bipolar diffusion charging of aerosol particles—I: experimental results within the diameter range 4–30 nm, Journal of Aerosol Science, 14, 671–677, https://doi.org/10.1016/0021-8502(83)90071-X, 1983.

Hyttinen, N., Otkjær, R. V., Iyer, S., Kjaergaard, H. G., Rissanen, M. P., Wennberg, P. O., and Kurtén, T.: Computational Comparison of Different Reagent Ions in the Chemical Ionization of Oxidized Multifunctional Compounds, J. Phys. Chem. A, 122, 269–279, https://doi.org/10.1021/acs.jpca.7b10015, 2018.

Ibarra, I., Rodríguez-Maroto, J., and Alonso, M.: Bipolar charging and neutralization of particles below 10 nm, the conditions to reach the stationary charge distribution, and the effect of a non-stationary charge distribution on particle sizing, Journal of Aerosol Science, 140, 105479, https://doi.org/10.1016/j.jaerosci.2019.105479, 2020.

ISO 15900:2020 - Determination of particle size distribution - Differential electrical mobility analysis for aerosol particles, 2020.

Jiang, J., Kim, C., Wang, X., Stolzenburg, M. R., Kaufman, S. L., Qi, C., Sem, G. J., Sakurai, H., Hama, N., and McMurry, P. H.: Aerosol Charge Fractions Downstream of Six Bipolar Chargers: Effects of Ion Source, Source Activity, and Flowrate, Aerosol Science and Technology, 48, 1207–1216, https://doi.org/10.1080/02786826.2014.976333, 2014.

Johnson, T. J., Nishida, R. T., Irwin, M., Symonds, J. P. R., Olfert, J. S., and Boies, A. M.: Measuring the bipolar charge distribution of nanoparticles: Review of methodologies and development using the Aerodynamic Aerosol Classifier, Journal of Aerosol Science, 143, 105526, https://doi.org/10.1016/j.jaerosci.2020.105526, 2020.

Johnson, T. J., Nishida, R. T., Zhang, X., Symonds, J. P. R., Olfert, J. S., and Boies, A. M.: Generating an aerosol of homogeneous, non-spherical particles and measuring their bipolar charge distribution, Journal of Aerosol Science, 153, 105705, https://doi.org/10.1016/j.jaerosci.2020.105705, 2021.

Kallinger, P., Steiner, G., and Szymanski, W. W.: Characterization of four different bipolar charging devices for nanoparticle charge conditioning, J Nanopart Res, 14, 944, https://doi.org/10.1007/s11051-012-0944-z, 2012.

Kangasluoma, J., Cai, R., Jiang, J., Deng, C., Stolzenburg, D., Ahonen, L. R., Chan, T., Fu, Y., Kim, C., Laurila, T. M., Zhou, Y., Dada, L., Sulo, J., Flagan, R. C., Kulmala, M., Petäjä, T., and Lehtipalo, K.: Overview of measurements and current instrumentation for 1–10 nm aerosol particle number size distributions, Journal of Aerosol Science, 148, 105584, https://doi.org/10.1016/j.jaerosci.2020.105584, 2020.

Kilpatrick, W. D.: An experimental mass-mobility relation for ions in air at atmospheric pressure, in: Proc. Annu. Conf. Massspectrosc, 320–325, 1971.

Kimoto, S., Mizota, K., and Adachi, M.: Theoretical and Experimental Evaluation of a Mixing-Type Bipolar Charger Using Corona-Discharge at High Pressure, J. Chem. Eng. Japan / JCEJ, 44, 535–545, https://doi.org/10.1252/jcej.10we305, 2011.

Knutson, E. O. and Whitby, K. T.: Accurate measurement of aerosol electric mobility moments, Journal of Aerosol Science, 6, 453–460, https://doi.org/10.1016/0021-8502(75)90061-0, 1975.

Kohno, J., Mafuné, F., and Kondow, T.: Cluster Ion Formation from Alcohol Solutions of CaI_2, J. Phys. Chem. A, 103, 1518–1522, https://doi.org/10.1021/jp983559i, 1999.

Kojima, H.: Measurements of Equilibrium Charge Distributions on Aerosols in Bipolar Ionic Atmosphere, 12, 2363–2368, 1978.

https://doi.org/10.5194/ar-2026-29
Preprint. Discussion started: 4 August 2026

Lee, H. M., Soo Kim, C., Shimada, M., and Okuyama, K.: Bipolar diffusion charging for aerosol nanoparticle measurement using a soft X-ray charger, Journal of Aerosol Science, 36, 813–829, https://doi.org/10.1016/j.jaerosci.2004.10.011, 2005.

Leppä, J., Mui, W., Grantz, A. M., and Flagan, R. C.: Charge distribution uncertainty in differential mobility analysis of aerosols, Aerosol Science and Technology, 51, 1168–1189, https://doi.org/10.1080/02786826.2017.1341039, 2017.

Li, L., Chahl, H. S., and Gopalakrishnan, R.: Comparison of the predictions of Langevin Dynamics-based diffusion charging collision kernel models with canonical experiments, Journal of Aerosol Science, 140, 105481, https://doi.org/10.1016/j.jaerosci.2019.105481, 2020.

Li, Y., Attoui, M., Liu, Y., Sun, Q., Li, Q., Cai, R., and Wang, L.: Size-resolved chemical composition analysis of ions produced by a dielectric barrier discharge bipolar charger, Journal of Aerosol Science, 189, 106623, https://doi.org/10.1016/j.jaerosci.2025.106623, 2025.

Liu, B. Y. H. and Pui, D. Y. H.: Electrical Neutralization of Aerosols, 5, 465–472, https://doi.org/10.1016/0021-8502(74)90086-X, 1974.

Liu, B. Y. H., Pui, D. Y. H., and Lin, B. Y.: Aerosol Charge Neutralization by a Radioactive Alpha Source, Particle & Particle Systems Characterization, 3, 111–116, https://doi.org/10.1002/ppsc.19860030304, 1986.

Liu, Y., Attoui, M., Yang, K., Chen, J., Li, Q., and Wang, L.: Size-resolved chemical composition analysis of ions produced by a commercial soft X-ray aerosol neutralizer, Journal of Aerosol Science, 147, 105586, https://doi.org/10.1016/j.jaerosci.2020.105586, 2020.

Maißer, A., Thomas, J. M., Larriba-Andaluz, C., He, S., and Hogan, C. J.: The mass–mobility distributions of ions produced by a Po-210 source in air, Journal of Aerosol Science, 90, 36–50, https://doi.org/10.1016/j.jaerosci.2015.08.004, 2015.

Mäkelä, J. M., Jokinen, V., Mattila, T., Ukkonen, A., and Keskinen, J.: Mobility distribution of acetone cluster ions, Journal of Aerosol Science, 27, 175–190, https://doi.org/10.1016/0021-8502(95)00560-9, 1996.

Marlow, W. H. and Brock, J. R.: Calculations of bipolar charging of aerosols, Journal of Colloid and Interface Science, 51, 23–31, https://doi.org/10.1016/0021-9797(75)90078-8, 1975.

Matsoukas, T.: The Coagulation Rate of Charged Aerosols in Ionized Gases, Journal of Colloid and Interface Science, 187, 474–483, https://doi.org/10.1006/jcis.1996.4723, 1997.

Melandri, C., Tarroni, G., Prodi, V., Zaiacomo, T. D., Formignani, M., and Lombard, C. C.: Deposition of Charged Particles in Human Airways, 14, 657–669, 1983.

Nishida, R. T., Johnson, T. J., Hassim, J. S., Graves, B. M., Boies, A. M., and Hochgreb, S.: A Simple Method for Measuring Fine-to-Ultrafine Aerosols Using Bipolar Charge Equilibrium, ACS Sens., 5, 447–453, https://doi.org/10.1021/acssensors.9b02143, 2020.

Nishida, R. T., Johnson, T. J., and Olfert, J. S.: On the three charge regimes of bipolar charge conditioners, Aerosol Science and Technology, 59, 499–520, https://doi.org/10.1080/02786826.2025.2461161, 2025.

Niskanen, M., Niskanen, M., Ursin, A., Ylisirniö, A., and Lehtinen, K. E. J.: Quantifying charger-related uncertainty in electrical mobility analysis of aerosols with MPSS-UQ 1.0, EGUsphere [preprint], https://doi.org/10.5194/egusphere-2026-2013, 2026.

Park, S. H., Lee, K. W., Shimada, M., and Okuyama, K.: Coagulation of bipolarly charged ultrafine aerosol particles, Journal of Aerosol Science, 36, 830–845, https://doi.org/10.1016/j.jaerosci.2004.10.013, 2005.

Reischl, G. P., Scheibel, H. G., and Porstendörfer, J.: The bipolar charging of aerosols: Experimental results in the size range below 20-nm particle diameter, Journal of Colloid and Interface Science, 91, 272–275, https://doi.org/10.1016/0021-9797(83)90332-6, 1983.

Reischl, G. P., Mäkelä, J. M., Karch, R., and Necid, J.: Bipolar charging of ultrafine particles in the size range below 10 nm, Journal of Aerosol Science, 27, 931–949, https://doi.org/10.1016/0021-8502(96)00026-2, 1996.

https://doi.org/10.5194/ar-2026-29
Preprint. Discussion started: 4 August 2026

Romay, F. J. and Pui, D. Y. H.: On the Combination Coefficient of Positive Ions with Ultrafine Neutral Particles in the Transition and Free-Molecule Regimes, Aerosol Science and Technology, 17, 134–147, https://doi.org/10.1080/02786829208959566, 1992.

Saputra, C., Kamil, A. I., Munir, M. M., Waris, A., and Novitrian: The performance of an electrical ionizer as a bipolar aerosol charger for charging ultrafine particles, Aerosol Science and Technology, 56, 117–133, https://doi.org/10.1080/02786826.2021.1976719, 2022.

Schmidt-Ott, F., Maisser, A., and Biskos, G.: Mass and Mobility of Ions Produced by Radioactive Sources and Corona Discharges, Anal. Chem., 96, 14405–14412, https://doi.org/10.1021/acs.analchem.4c01796, 2024.

Steiner, G. and Reischl, G. P.: The effect of carrier gas contaminants on the charging probability of aerosols under bipolar charging conditions, Journal of Aerosol Science, 54, 21–31, https://doi.org/10.1016/j.jaerosci.2012.07.008, 2012.

Steiner, G., Jokinen, T., Junninen, H., Sipilä, M., Petäjä, T., Worsnop, D. R., Reischl, G., and Kulmala, M.: High-Resolution Mobility and Mass Spectrometry of Negative Ions Produced in a 241Am Aerosol Charger, Aerosol Science and Technology, 48, 261–270, https://doi.org/10.1080/02786826.2013.870327, 2014.

Stober, J., Schleicher, B., and Burtscher, H.: Bipolar Diffusion Charging of Particles in Noble Gases, Aerosol Science and Technology, 14, 66–73, https://doi.org/10.1080/02786829108959471, 1991.

Tigges, L., Jain, A., and Schmid, H.-J.: On the bipolar charge distribution used for mobility particle sizing: Theoretical considerations, Journal of Aerosol Science, 88, 119–134, https://doi.org/10.1016/j.jaerosci.2015.05.010, 2015.

Timko, M. T., Yu, Z., Kroll, J., Jayne, J. T., Worsnop, D. R., Miake-Lye, R. C., Onasch, T. B., Liscinsky, D., Kirchstetter, T. W., Destaillats, H., Holder, A. L., Smith, J. D., and Wilson, K. R.: Sampling Artifacts from Conductive Silicone Tubing, Aerosol Science and Technology, 43, 855–865, https://doi.org/10.1080/02786820902984811, 2009.

Tu, G., Song, Q., and Yao, Q.: Relationship between particle charge and electrostatic enhancement of filter performance, Powder Technology, 301, 665–673, https://doi.org/10.1016/j.powtec.2016.06.044, 2016.

Ungethüm, E.: The mobilities of small ions in the atmosphere and their relationship, 25–37, 1974.

Vemury, S. and Pratsinis, S. E.: Charging and coagulation during flame synthesis of silica, Journal of Aerosol Science, 27, 951–966, https://doi.org/10.1016/0021-8502(96)00040-7, 1996.

Vincent, J. H.: On the practical significance of electrostatic lung deposition of isometric and fibrous aerosols, Journal of Aerosol Science, 16, 511–519, https://doi.org/10.1016/0021-8502(85)90003-5, 1985.

Whitby, K. T.: Generator for Producing High Concentrations of Small Ions, Review of Scientific Instruments, 32, 1351–1355, https://doi.org/10.1063/1.1717250, 1961.

White, H. J.: Particle Charging in Electrostatic Precipitation, Transactions of the American Institute of Electrical Engineers, 70, 1186–1191, https://doi.org/10.1109/T-AIEE.1951.5060545, 1951.

Wiedensohler, A.: An approximation of the bipolar charge distribution for particles in the submicron size range, Journal of Aerosol Science, 19, 387–389, https://doi.org/10.1016/0021-8502(88)90278-9, 1988.

Wiedensohler, A. and Fissan, H. J.: Bipolar Charge Distributions of Aerosol Particles in High-Purity Argon and Nitrogen, Aerosol Science and Technology, 14, 358–364, https://doi.org/10.1080/02786829108959498, 1991.

Wiedensohler, A., Lütkemeier, E., Feldpausch, M., and Helsper, C.: Investigation of the bipolar charge distribution at various gas conditions, Journal of Aerosol Science, 17, 413–416, https://doi.org/10.1016/0021-8502(86)90118-7, 1986.

Yu, Y., Liz Alexander, M., Perraud, V., Bruns, E. A., Johnson, S. N., Ezell, M. J., and Finlayson-Pitts, B. J.: Contamination from electrically conductive silicone tubing during aerosol chemical analysis, Atmospheric Environment, 43, 2836–2839, https://doi.org/10.1016/j.atmosenv.2009.02.014, 2009.